



HAL
open science

Experimental characterization of the mechanical behaviour and the failure of multi-sheet and multi-material spot welded assembly

Rami Tounsi, Grégory Haugou, Fahmi Chaari, Nicolas Leconte, Eric Markiewicz

► To cite this version:

Rami Tounsi, Grégory Haugou, Fahmi Chaari, Nicolas Leconte, Eric Markiewicz. Experimental characterization of the mechanical behaviour and the failure of multi-sheet and multi-material spot welded assembly. *International Journal of Impact Engineering*, 2019, 130, pp.226-238. 10.1016/j.ijimpeng.2019.04.017 . hal-03448674

HAL Id: hal-03448674

<https://uphf.hal.science/hal-03448674v1>

Submitted on 20 Dec 2021

HAL is a multi-disciplinary open access archive for the deposit and dissemination of scientific research documents, whether they are published or not. The documents may come from teaching and research institutions in France or abroad, or from public or private research centers.

L'archive ouverte pluridisciplinaire **HAL**, est destinée au dépôt et à la diffusion de documents scientifiques de niveau recherche, publiés ou non, émanant des établissements d'enseignement et de recherche français ou étrangers, des laboratoires publics ou privés.



Distributed under a Creative Commons Attribution - NonCommercial 4.0 International License

Experimental characterization of the mechanical behaviour and the failure of multi-sheet and multi-material spot welded assembly

R. Tounsi^a, G. Haugou^a, F. Chaari^a, N. Leconte^a, E. Markiewicz^{a,*}

^a *Univ. Polytechnique Hauts-de-France, CNRS, UMR 8201 - LAMIH, F-59313 Valenciennes, France*

Abstract

An experimental investigation of the mechanical behaviour of three-sheet multi-material spot welded assembly is performed. An experimental device based on the Arcan principle is developed to test the three-sheet spot welded specimen under pure opening mode, pure shear mode and mixed opening/shear mode with three nugget sizes. A significant effect of the loading angle is reported and explained by three identified failure modes as a pull-out failure mode (pure opening), an inter-facial failure mode (pure shear) and a mixed pull-out/inter-facial failure mode (mixed opening/shear). A pronounced effect of nugget diameter size is reported on the ultimate force and the dissipated energy. A preliminary study of the strain-rate sensitivity of the three-sheet multi-material spot welded assembly is also undertaken.

Keywords:

Spot welds, Multi-sheet, Multi-material, Experiments, Dynamic testing

1. Introduction

Reducing the weight in the automotive industry improves fuel efficiency and reduces greenhouse gas emissions, but the mechanical strength required

*Corresponding author

Email addresses: tounsi.f@gmail.com (R. Tounsi), gregory.haugou@uphf.fr (G. Haugou), fahmi.chaari@uphf.fr (F. Chaari), nicolas.leconte@uphf.fr (N. Leconte), eric.markiewicz@uphf.fr (E. Markiewicz)

Preprint submitted to International Journal of Impact Engineering

April 14, 2019

4 to meet crash safety requirements has to be maintained. The weight reduction
5 is achieved through the increasing development and use of lightweight materials
6 or by reducing the sheet thicknesses made of Ultra High Strength Steels (UHSS).
7 Up to now, Resistance Spot Welding (RSW) remains the most commonly used
8 (and the cheaper) process to join two or more sheets (around four thousands
9 spot welds are performed to assemble the body in white).

10 Using this RSW process, it is possible and easy to joint different steel
11 grades combinations and sheet thicknesses. Joining multi-sheet (more than
12 two) by RSW is considered in this study. Compared to two-sheet spot welded
13 assemblies, joining multi-sheet is significantly more complicated. Indeed, the
14 use of different steel grades combinations and different sheet thicknesses in the
15 multi-layer spot welded assemblies complicates not only the welding process but
16 also the investigation of their mechanical behaviour up to failure that represents
17 a new challenge. Despite the increasing use of this new generation of RSW, their
18 mechanical behaviour is not yet well studied. To the knowledge of the authors,
19 most of the published works consider two-sheet spot welded assemblies.

20 Since 1958, mechanical tests have been discussed [1, 2, 3] in particular for
21 pure tension, tension-shear and peel specimens. For these types of tests, a large
22 part of the sheet sample deforms plastically, in particular far from the spot weld.
23 Thus, it contributes significantly to the global behaviour. Moreover, it is difficult
24 to express the failure properties because the tensile/shear load ratio conditions
25 vary during the test. More recently, many researchers [4, 5, 6, 7, 8, 9] have
26 proposed to adapt the Arcan tests to investigate the failure characteristics of
27 two-sheet spot welded assemblies under combined loading conditions. Indeed,
28 Arcan tests have advantages over standard tests that the plates contribution
29 around the weld nugget in the mechanical response is reduced. Moreover, it
30 allows tensile (mode I) and shear (mode II) loads to be pure or combined and
31 well controlled. However, these devices are characterized by a large mass that
32 generates inertial forces during the dynamic loading. Thus, they can be used
33 only under quasi-static loading conditions. To overcome this limitation and
34 to investigate the strain rate sensitivity of spot welds in dynamic conditions,

35 Langrand and Markiewicz [8] have proposed an experimental device with a
36 reduced mass to cope with these inertial forces.

37 The published experimental studies previously presented are limited to two-
38 sheet spot welded assemblies. However, the mechanical behaviour of the multi-
39 sheet, multi-steel grades spot-welded assemblies is not yet well studied. Few
40 works relate the study of the mechanical strength under quasi-static loading
41 using conventional tensile-shear specimens. In fact, Pouranvari et al. [10, 11]
42 and Tavasolizadeh et al. [12] have been interested in the nugget growth,
43 mechanical performance and failure behavior of three-sheet low carbon steel
44 resistance spot welds. Nielsen et al. [13] have investigated the weldability of
45 a thin, low-carbon steel sheet to high-strength low-alloy (HSLA) and AHSS.
46 Recently, Wei et al. [14] have studied the weldability and mechanical properties
47 of similar and dissimilar resistance spot welds of three-layer advanced high
48 strength steels. All these works have used the tensile-shear tests to study
49 the mechanical behaviour of three-sheet spot welded assemblies. This type
50 of experimental specimen is characterized by an important contribution of
51 the plates in the global response. In this context, an advanced experimental
52 procedure based on Arcan test is proposed in this work to characterize the
53 mechanical behaviour of a three-sheet spot welded assembly made of a thin low-
54 carbon steel sheet and two thicker UHSS sheets. The proposed device allows
55 the investigation of the spot welded assembly under pure and combined modes
56 I/II loading conditions. Thus, the loading modes I/II are combined and well
57 controlled, with a reduced contribution of the plates strength surrounding the
58 weld nugget in the macroscopic response. The mechanical behaviour, the failure
59 modes and the strain-rate sensitivity of this multi-sheet and multi-steel grades
60 spot-welded assembly are investigated.

61 The first section presents the studied three-sheet spot welded assembly and
62 the proposed experimental device. The experimental results are presented in
63 the second section. In the third section, the influences of the loading angle
64 and the nugget size on the mechanical behaviour of the three-sheet spot welded
65 assembly are discussed. Based on the experimental results, the parameters of

66 a macroscopic force-based failure criterion dedicated to FE crash modelling are
67 identified. Finally, as a first attempt, the strain rate sensitivity of the spot
68 welded assembly is discussed in the fourth section.

69 **2. Experimental characterization of the mechanical behaviour of** 70 **three-sheet multi-steel grades spot welded assembly**

71 *2.1. Studied spot weld specimens*

72 The studied spot welded assembly consists of three sheets and involves two
73 steel grades: (P1) is 2 mm thick and made of 22MnB5 ultra-high strength steel,
74 (P2) is 0.65 mm thick and made of DX54D mild steel and (P3) is 1.6 mm thick
75 and made of 22MnB5 (figure 1). The DX54D mild steel grade is classified as an
76 alloy quality low carbon steel. The 22MnB5 is classified as ultra-high strength
77 steel. It is considered as an efficient way to combine the superior mechanical
78 properties, weight/cost reduction and crash safety. This kind of steel grade is
79 intended for structural parts and safety in the automotive sector. Two metallic
80 rigs have been designed and joined each free face of the spot welded assembly
81 (figure 1). The role of the two rigs is to ensure the connection between the spot
82 welded specimen and the device. These rigs are made of Z160 steel alloy, and
83 are 6 mm thick. They are rigidly linked to the free faces of the sample by a
84 process wich is not detailed in this paper due to a confidentiality agreement
85 with our industrial partner. The mechanical strength of this connection has
86 been experimentally checked to be higher than the spot weld one. In addition,
87 this connection ensures an isotropic loading of the spotweld. [8]

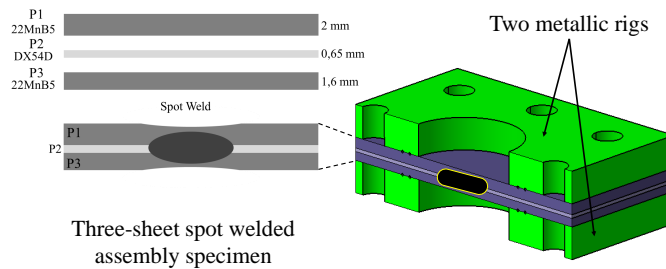


Figure 1: Studied spot welded specimen

88 The spot welding process was performed by our industrial partner according
 89 to his know-how. Depending on the welding conditions, different weld nugget
 90 sizes are possible according to internal quality rules. According to internal rules
 91 criteria, the spot welds are classified in two ranges: Acceptable Nugget and
 92 Not Acceptable Nugget. Figure 2 shows the classification of the spot weld in
 93 accordance with Nugget size.

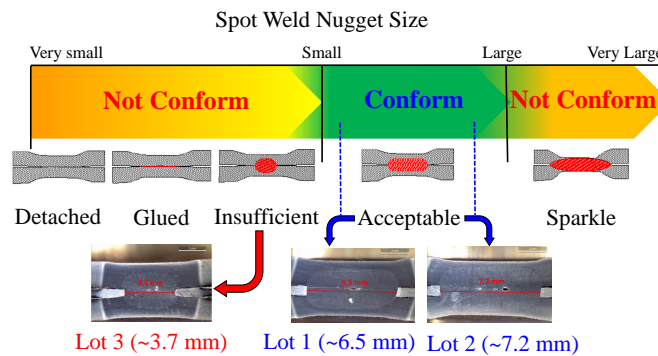


Figure 2: Spot welds quality according to the nugget size and the three considered Lots

94 In this study, three lots (figure 2) are considered as follows :

- 95
- Lot 1 : Acceptable Nugget (Nugget Conform A small size);

- 96 • Lot 2 : Acceptable Nugget (Nugget Conform B large size);
- 97 • Lot 3 : Not Acceptable Nugget (Nugget Not Conform C).

98 According to the different loading conditions, three types of specimens
 99 are proposed to perform three loading configurations. The first configuration
 100 called "Configuration 1-3" corresponds to spot weld specimen "S.1-3" composed
 101 by three square plates (60 mm x 60 mm). The second configuration called
 102 "Configuration 1-2" corresponds to spot weld specimen "S.1-2" composed by
 103 two square plates (P1 and P2 : 60 mm x 60 mm) and a circle plate (P3 : 25
 104 mm). The third configuration is the inverse of the second configuration called
 105 "Configuration 2-3" corresponds to spot weld specimen "S.2-3" composed by a
 106 circle plate (P1 : 25 mm) and two square plates (P2 and P3 : 60 mm x 60 mm).
 107 Figure 3 presents a schematization of the specimen different configurations.

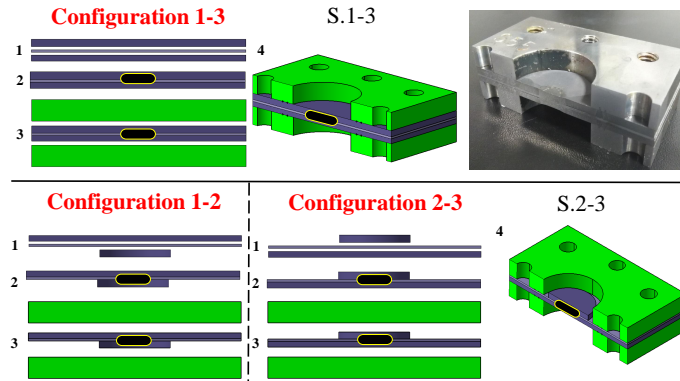


Figure 3: Loading configurations 1-3, 1-2 and 2-3

108 2.2. Experimental device

109 An experimental device based on the Arcan principle is developed to
 110 investigate the three-sheet spot welded specimen behaviour and failure modes
 111 in pure and combined loading conditions. The proposed device is composed by
 112 rigid counterparts that have been designed for each angular position as presented
 113 in figure 4. By convention, the pure tension (opening mode) is obtained for $\psi =$
 114 0° , and on the other end of range, the pure shear for $\psi = 90^\circ$. The specimen is

115 positioned on the device by two centring pins and fixed with six screws (figure
116 4).

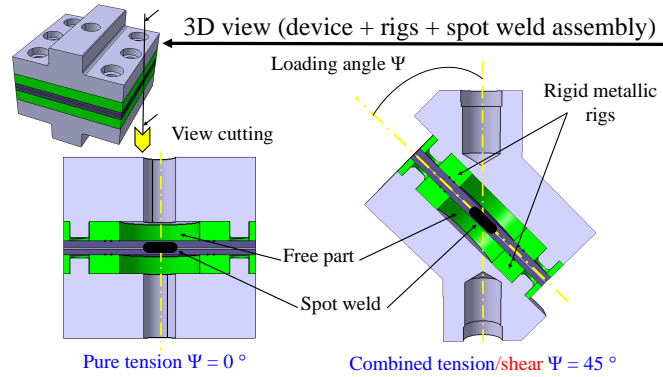


Figure 4: The proposed device with the studied specimen "three-sheet spot welded assembly + two rigid metallic rigs"

117 The geometry of the experimental device has been designed thanks to FE
118 simulations using approximate material data. On the one hand, the linear
119 dynamics response is simulated to ensure that natural frequencies will be avoided
120 for the considered loading velocities. On the other hand, all mechanical design
121 for the number and the location of the screws, the thickness of the counterparts,
122 is accomplished thanks to numerical simulations. The choice of the load cell is
123 also based on the obtained results. The final design realises a compromise
124 between mechanical strength and reduced inertia effects (Figure 5).

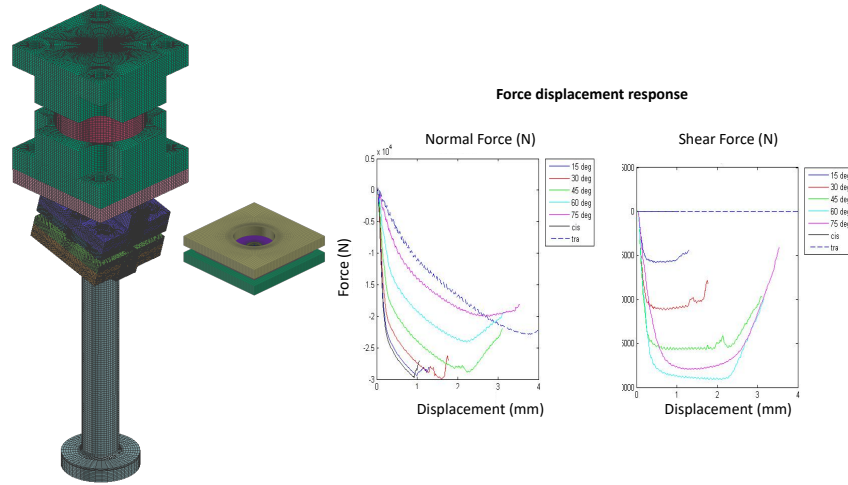


Figure 5: Overview of FE simulations carried out

125 The tests are carried out on a high speed hydraulic machine (INSTRON
 126 VHS 65/20). In a first step, only quasi-static loading conditions are applied on
 127 the specimens. The hydraulic actuator moves along the vertical axis (z) with a
 128 loading speed of $V = 0.001m/s$. The forces along the three main directions of
 129 the machine (F_x ; F_y and F_z) are recorded during experiments by using a tri-
 130 axial load cell (Kistler 9367C). The load cell links the upper part of the device
 131 to the hydraulic machine with four screws. The rotations are not permitted.
 132 The bottom part of the device is connected to the hydraulic actuator by a stiff
 133 rod. The actuator is initially not in contact with the stiff rod. This contact is
 134 only established when the actuator reaches its target velocity. In quasi static
 135 loading, the velocity remains constant during all the test, until the failure of
 136 the specimen. Figure 6 shows raw data for typical force and displacement
 137 measurements. However, for higher loading velocities, it becomes more difficult
 138 to keep the closed loop regulation of the actuator due to the relative brittle
 139 behaviour of the considered spot weld.

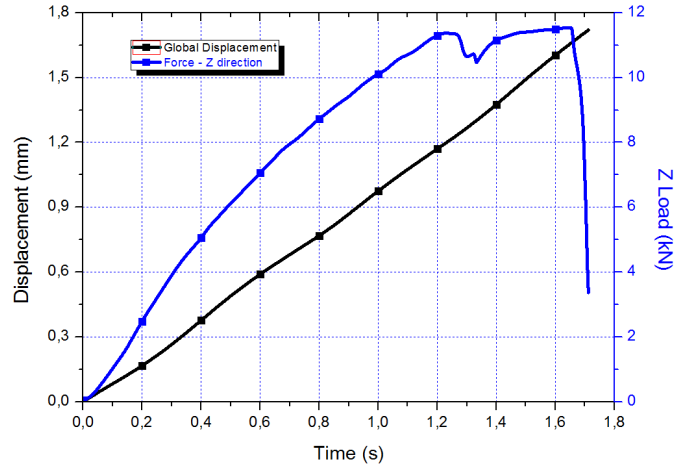


Figure 6: Typical raw data on high speed hydraulic machine

140 The displacement is measured by a LVDT sensor **in the vertical direction**,
 141 with a measurement range equal to 300 mm and an error of 0.15 mm. Figure 7
 142 shows the complete set up used for the experiments.

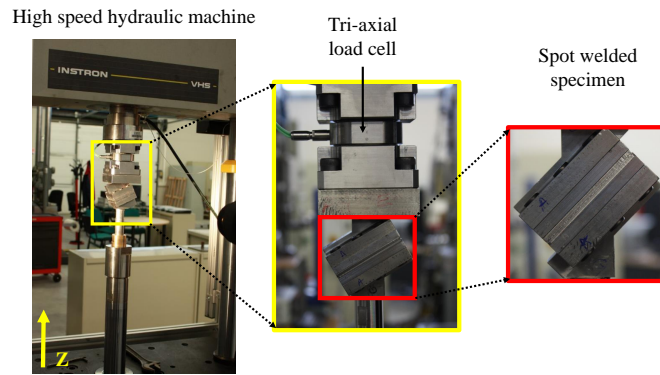


Figure 7: Experimental set-up for testing spot-welded specimens

143 A special set-up is designed for centring the spot weld assembly with the free
 144 zone center to ensure that the principal axe of the spot weld is collinear with the
 145 loading direction. The small tolerances imposed to manufacture the specimen

146 allow to neglect the bending moments. It has been verified that in plane X and
 147 Y force components are not significant compared to vertical Z force component.
 148 This is illustrated in Figure 8 where the three force components are measured.

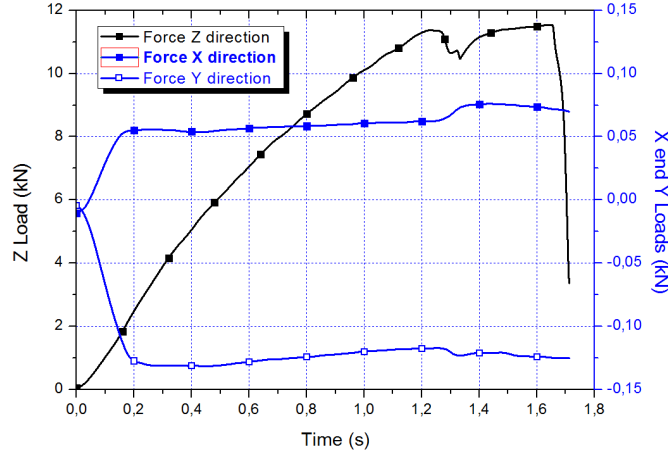


Figure 8: Typical XYZ force components measured with the tri-axial load cell obtained for $\psi = 45^\circ$

149 Thus, only a resultant force F is considered at the center of the specimen.
 150 The normal (N) and shear (T) force components can be expressed with respect
 151 to the loading angle ψ (Eqs. 1 and 2).

$$N(t) = F(t) * \cos(\psi) \quad (1)$$

152 and

$$T(t) = F(t) * \sin(\psi) \quad (2)$$

153 3. Experimental results

154 To study the mechanical behaviour and the failure of the three-sheet multi-
 155 steel grades spot welded assembly, three possible configurations (1-2), (2-3) and
 156 (1-3) have been tested.

157 *3.1. Configurations (1-2) and (2-3)*

158 Preliminary experimental results suggest that the mechanical behaviour of
 159 the studied three-sheet spot weld assemblies (S.1-2 and S.2-3) are similar for the
 160 configurations "1-2" and "2-3". In fact, for both configurations the experimental
 161 response corresponds mainly to the behaviour of the middle plate made of
 162 DX54D mild steel, because the thick plates made of 22MnB5 UHSS are much
 163 more rigid compared to the plate made of DX54D. This remark holds true for
 164 the pure tensile, pure shear and mixed mode $\psi = 45^\circ$. Thus, in the following
 165 only the experimental results of configuration "1-2" are considered.

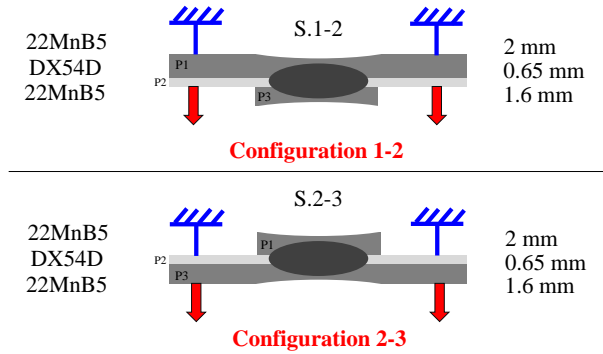


Figure 9: "1-2" and "2-3" configurations

166 The analysis of the failure mode for $\psi < 90^\circ$ in configuration 1-2 shows that
 167 the spot weld is not loaded (figure 10) and that the failure of the assembly is
 168 caused by the punching of the middle plate (DX54D) by the circle top plate P_3
 169 made of 22MnB5. Therefore, only the shear pure mode ($\psi = 90^\circ$) is considered
 170 for the configuration "1-2". Figure 11 shows the failure mode of the considered
 171 test.

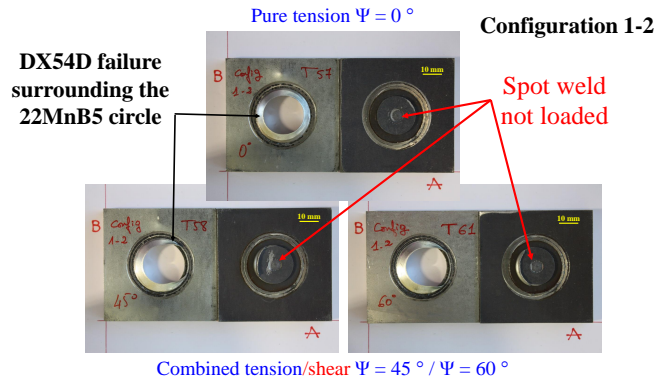


Figure 10: Failure modes for the pure opening test ($\psi = 0^\circ$) and for mixed I/II modes ($\psi = 45^\circ$ and $\psi = 60^\circ$) in configuration "1-2"

172 As shown in figure 12, for $\psi = 90^\circ$ in the configuration 1-2, the force
 173 increases progressively with the displacement until a maximum value of force is
 174 reached. Then, a progressive decrease of the load is observed up to complete
 175 failure.

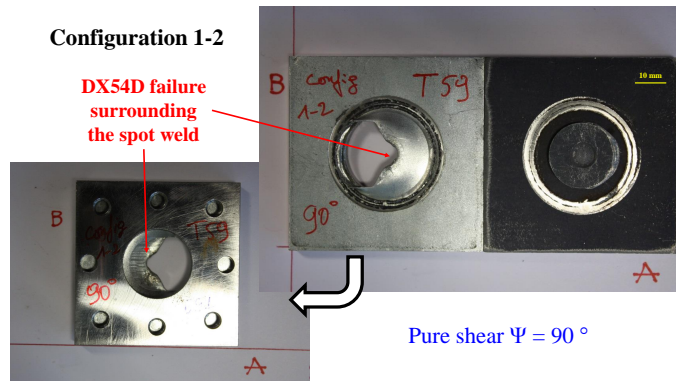


Figure 11: Failure mode for the pure shear test in configuration "1-2" ($\psi = 90^\circ$)

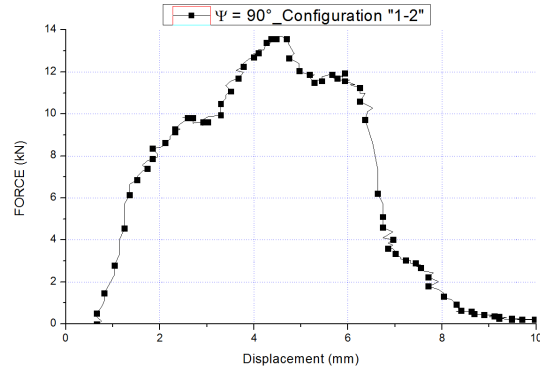


Figure 12: Force vs. displacement for the pure shear test in configuration "1-2" ($\psi = 90^\circ$)

176 3.2. Configuration (1-3)

177 Considering the configuration "1-3", five loading angles have been considered
 178 in this investigation: $\psi = 0^\circ$ for the pure opening mode, $\psi = 30^\circ$, $\psi = 45^\circ$,
 179 $\psi = 60^\circ$ for the mixed I/II modes and $\psi = 90^\circ$ for the pure shear mode. A
 180 set of three tests has been performed for each loading configuration. A good
 181 reproducibility is checked and the dispersions are not significant. So, the mean
 182 value of the three responses is calculated.

183 3.2.1. Force-displacement responses

184 Figure 13 shows a typical force vs. displacement response of three-sheet spot
 185 welded assembly. The response may be divided into three phases, which can be
 186 described as follows:

- 187 • Phase 1 : characterised by an elastic-plastic response of the spot weld;
- 188 • Phase 2 : an ultimate force is reached;
- 189 • Phase 3 : sudden or progressive failure of the assembly depending on the
 190 loading angle.

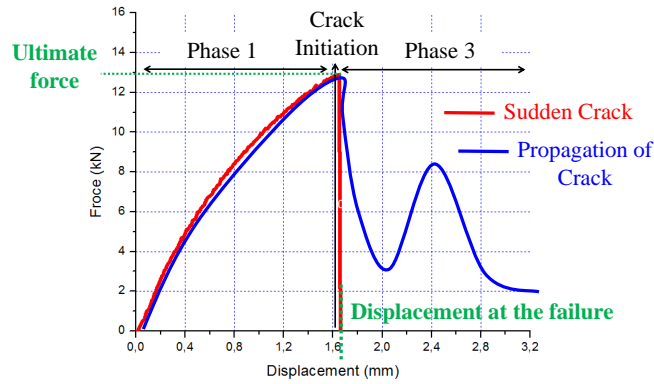


Figure 13: Typical force vs. displacement response of three-sheet spot weld assembly

191 The force vs. displacement are reported for all Lots (Lot 1, Lot 2 and Lot 3).
 192 The experimental responses have similar shape. For this reason, only responses
 193 for Lot 1 are presented in this section. A discussion on the nugget quality and
 194 diameter size effects is realised in the section (4.2). Figure 14 presents force
 195 vs. displacement responses for each loading angle ψ : pure opening mode, pure
 196 shear mode and mixed opening/shear mode (Lot 1 / configuration "1-3").

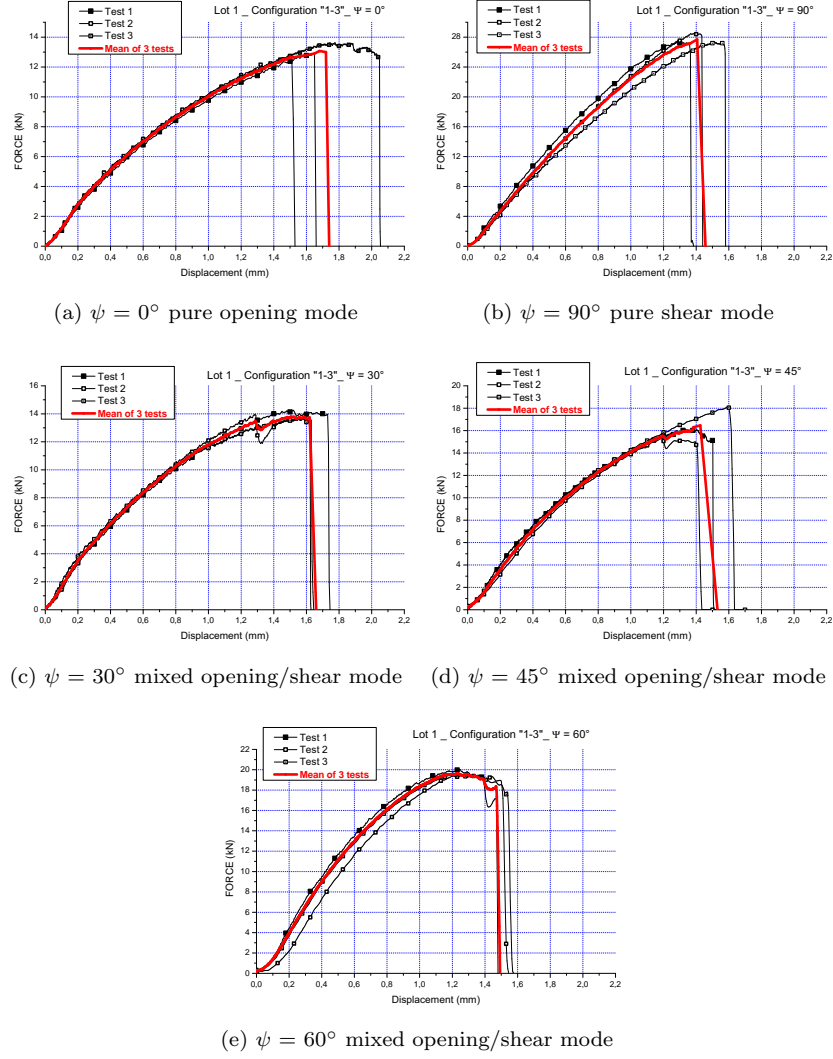


Figure 14: Force vs. displacement responses for pure opening mode (a) $\psi = 0^\circ$, pure shear mode (b) $\psi = 90^\circ$ and mixed opening/shear mode (c) $\psi = 30^\circ$, (d) $\psi = 45^\circ$, (e) $\psi = 60^\circ$

197 Based on the experimental responses presented in figure 14, the mean
 198 ultimate force and the relative average dispersion are calculated as follows :

$$\bar{F}_{Ultimate} = \frac{1}{n} \sum_i^n F_{Ultimate}(i), n = 3 \quad (3)$$

199 and

$$200 \text{ Coefficient of mean deviation : } \bar{D}(\%) = \frac{1}{n} \sum_i^n \left| \frac{F_{Ultimate}(i) - \bar{F}_{Ultimate}}{\bar{F}_{Ultimate}} \right| \times 100, n = 3 \quad (4)$$

200 Table 1 presents the mean ultimate force for different loading angle.

Table 1: Ultimate forces for different loading angles

	Pure opening	Mixed opening/shear			Pure shear
	$\psi = 0^\circ$	$\psi = 30^\circ$	$\psi = 45^\circ$	$\psi = 60^\circ$	$\psi = 90^\circ$
Test 1 (kN)	12.87	14.25	16.18	21.45	27.29
Test 2 (kN)	12.79	13.96	15.12	19.35	28.46
Test 3 (kN)	13.62	13.70	18.08	19.46	27.38
$\bar{F}_{Ultimate}$ (kN)	13.09	13.97	16.46	20.08	27.71
\bar{D} (%)	2.68	1.33	6.56	4.52	1.8

201 The mean displacement at failure and the dissipated energy coupled with the
 202 relative average dispersion are also calculated using the equations Eqs.3 and 4
 203 applied to the displacement and energy. The results are presented in tables 2
 204 and 3, respectively.

Table 2: Displacement at failure for different loading angles

	Pure opening	Mixed opening/shear			Pure shear
	$\psi = 0^\circ$	$\psi = 30^\circ$	$\psi = 45^\circ$	$\psi = 60^\circ$	$\psi = 90^\circ$
Test 1 (mm)	1.65	1.74	1.50	1.41	1.37
Test 2 (mm)	1.51	1.63	1.45	1.51	1.44
Test 3 (mm)	2.05	1.62	1.65	1.54	1.58
$\bar{U}_{Failure}$ (mm)	1.74	1.66	1.53	1.49	1.46
\bar{D} (%)	17.5	2.94	5.14	3.42	5.31

Table 3: Dissipated energy for different loading angles

	Pure opening	Mixed opening/shear			Pure shear
	$\psi = 0^\circ$	$\psi = 30^\circ$	$\psi = 45^\circ$	$\psi = 60^\circ$	$\psi = 90^\circ$
Test 1(kN.mm)	13.08	16.58	13.56	19.48	22.19
Test 2(kN.mm)	11.90	15.20	15.98	18.85	23.13
Test 3(kN.mm)	18.80	15.02	18.45	20.52	25.38
$\bar{E}_{Dissipated}$ (kN.mm)	14.59	15.60	16.13	19.70	23.56
\bar{D} (%)	19.22	4.20	9.50	3.06	5.12

205 The analysis of tables 1, 2 and 3 suggests that the relative average dispersion
 206 is fairly low for the ultimate forces ($< 7\%$ for $\psi = 45^\circ$). It is similar for the
 207 displacement at failure ($< 6\%$ for all cases except for $\psi = 0^\circ$). Therefore,
 208 a good reproducibility in terms of dissipated energy is reported with a relative
 209 average dispersion $< 10\%$ that is an acceptable deviation and allows to valid the
 210 reproducibility for the test. This dispersion could be explained by the variation
 211 of the diameter size nugget and the quality of the spot weld nugget related to
 212 the welding procedure for the same Lot (Lot 1). Moreover, eccentricity defects
 213 between the center of the spot weld and the free zone center are identified for
 214 some tested specimens. Despite the weak tolerances imposed to manufacture the
 215 spot weld assembly, eccentricity defects could be important for some specimen
 216 15.

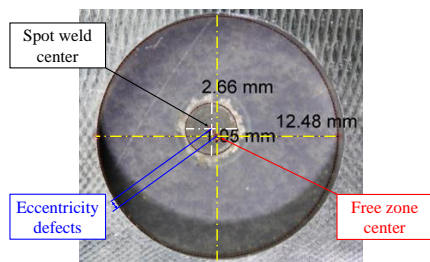


Figure 15: Illustration of an extreme eccentricity defect observed on a spot weld specimen

217 3.2.2. Failure modes

218 The post-mortem observations of the tested specimens allow to identify three
 219 principal failure modes according to the loading angle:

220 **Pull-out failure mode (M1):** For this mode the failure occurs around the
 221 spot weld nugget. This failure mode is obtained in the pure opening mode
 222 where the normal load is dominant during the test. The normal load
 223 generates a stress concentration around the nugget that creates a crack.
 224 The crack occurs due to necking/shearing throughout the thickness of the
 225 Base Material (BM) near the Heat-Affected Zone (HAZ) and propagates
 226 around the outline of the nugget. Thus, the weld nugget is pulling out
 227 from the P3 layer (22MnB5, thickness 1.6 mm). Figure 16 shows the
 228 section cut view of failed spot welds (post-mortem specimen) for the pure
 229 opening mode ($\psi = 0^\circ$).

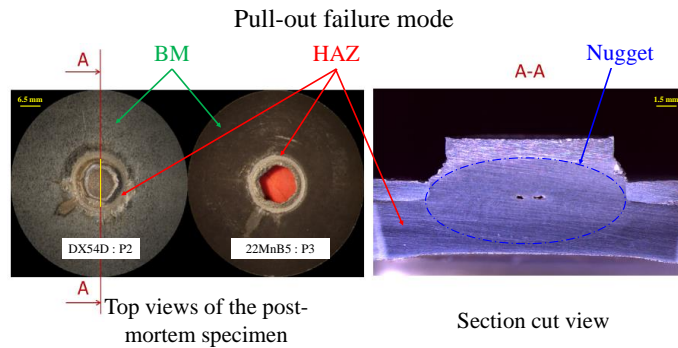


Figure 16: Pull-out failure mode of three-sheet spot weld for opening mode ($\psi = 0^\circ$)

230 **Inter-facial failure mode (M2):** This failure mode occurs when the shear
 231 load is dominant during test. The shear load generates a stress
 232 concentration at the sheet/sheet interface in the nugget level and leads to
 233 create an inter-facial crack that propagates through the spot weld
 234 as shown in figure 17 that presents a section cut view of failed spot welds
 235 (post-mortem specimen) for the pure shear mode ($\psi = 90^\circ$). Thus, the
 236 inter-facial mode occurs at the interface between the DX54D sheet metal
 237 (P2) and the thinnest thickness of the 22MnB5 sheets metal (P3).

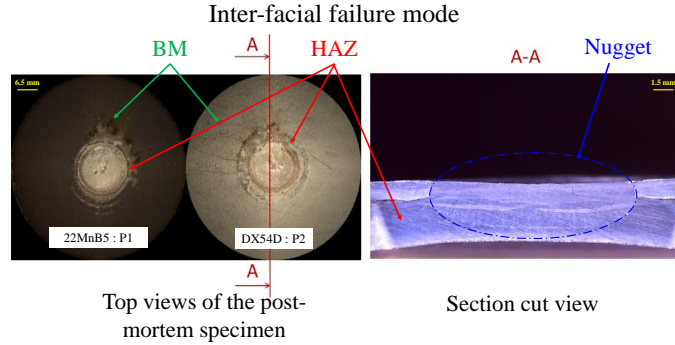


Figure 17: Inter-facial failure mode of three-sheet spot weld for shear mode ($\psi = 90^\circ$)

238 **Mixed Pull-out/Inter-Facial failure mode (M3):** It is a combination of
 239 the two previous presented failure modes as Pull-out/Inter-facial mode.
 240 This mode of failure occurs in the mixed opening/shear mode where
 241 the normal and shear loads are combined during test. The combined
 242 loads generate a stress concentration at the spot weld nugget that causes
 243 the deformation of the nugget at its mid thickness following the loading
 244 direction. Therefore, the principal axis of the nugget remains almost
 245 collinear with the loading direction. Thus, the normal load increases
 246 and becomes more dominant than the shear load. The opening mode
 247 conditions came back and lead to the pull out of the deformed weld nugget
 248 from the thinnest thickness of the 22MnB5 sheets metal (P3). After this
 249 last phase, the deformed nugget can interact with the central sheet leading
 250 to the progressive opening observed in figure 19. In fact, the post peak
 251 force is due to the plastic bending of the central sheet.

252 Figure 18 illustrates the observed mixed failure mode through a section
 253 cut view of failed spot weld (post-mortem specimen) for the mixed
 254 opening/shear mode $\psi = 60^\circ$.

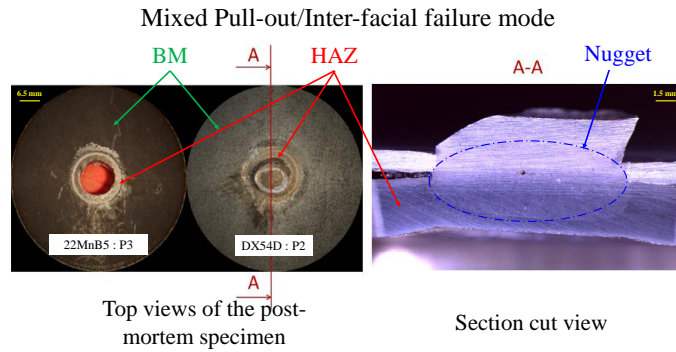


Figure 18: Mixed Pull-out/Inter-facial failure mode of three-sheet spot weld for mixed opening/shear mode ($\psi = 60^\circ$)

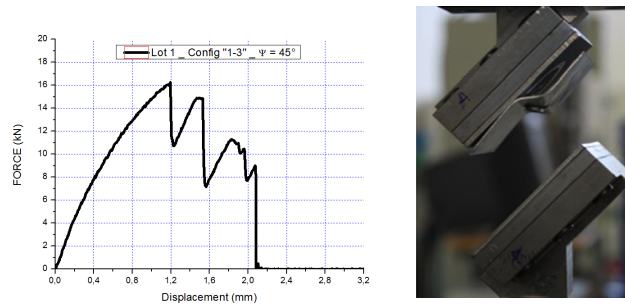


Figure 19: Typical force vs. displacement response of three-sheet spot weld assembly

255 Table 4 presents the different failure modes observed for different loading
 256 angles.

Table 4: Failure modes for different loading angles

Failure Mode	Pure opening	Mixed opening/shear			Pure shear
	$\psi = 0^\circ$	$\psi = 30^\circ$	$\psi = 45^\circ$	$\psi = 60^\circ$	$\psi = 90^\circ$
	M1	M1	M3	M3	M2

257 As a conclusion, three principal failure modes as Pull-out, Inter-facial and

258 Mixed Pull-out/Inter-facial are identified during experiments. The occurrence
 259 of such a mode is related to the loading conditions (pure opening, pure shear
 260 and mixed opening/shear). For a better understanding for these failure modes,
 261 Vickers hardness mapping test was performed on a specimen cut perfectly in
 262 the spot weld nugget center. A Future Tech Hardness Tester (Model FM) was
 263 used with a loading force of 300 g. The hardness distribution results allows
 264 to identify three characteristic zones of spot weld: Nugget, Heat Affected Zone
 265 (HAZ) and Base Material (BM) (Figure 20). A mapping step of 1 mm is used
 266 for the base material and 0.1 mm is used for the HAZ and the nugget.

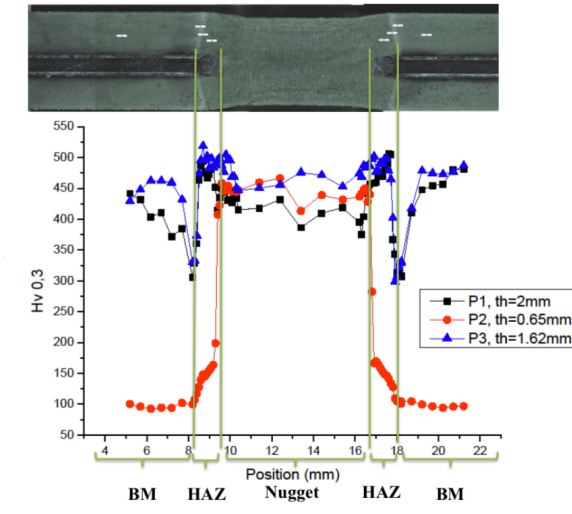


Figure 20: Hardness distribution along the spot weld joint assembly

267 **4. Discussion of the experimental results**

268 The analysis of the mechanical behaviour and the failure modes of the
 269 studied three-sheet spot welded assembly in the different loading conditions
 270 allows to investigate the influence of the loading angle and the effect of the
 271 nugget quality (nugget diameter size) on the ultimate force, the displacement
 272 at failure and the dissipated energy.

273 4.1. Effect of the loading angle

274 Based on the obtained results (Tabs. 1 and 2), the mean ultimate force
 275 ($\bar{F}_{Ultimate}$) vs. the loading angle (ψ) is presented in figure 21. The mean
 276 ultimate force increases exponentially. Indeed, between $\psi = 0^\circ$ and $\psi = 30^\circ$ the
 277 force is almost constant. Beyond of $\psi = 45^\circ$, a significant increase of the force is
 278 reported to reach the maximum of $\bar{F}_{Ultimate} = 27.71kN$ for $\psi = 90^\circ$. However,
 279 considering the mean displacement at the failure, figure 21 (b) shows that it
 280 decreases when the loading angle increases contrary to the ultimate force. The
 281 minimum mean displacement at failure $\bar{U}_{Ultimate} = 1.46mm$ is reached for the
 282 loading angle $\psi = 90^\circ$.

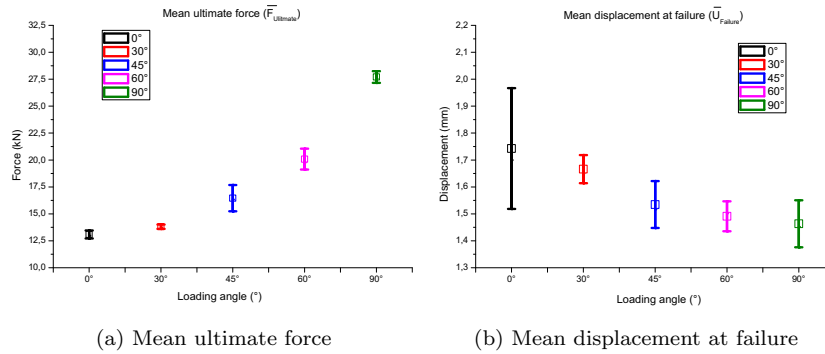


Figure 21: Effect of the loading angle ψ (a) Mean ultimate force and (b) Mean displacement at failure

283 The mean dissipated energy vs. the loading angle is presented in figure
 284 22.a The mean dissipated energy increases with the loading angle. Indeed, the
 285 failure for the pure shear mode requires an important quantity of energy when
 286 compared to the failure mode for the pure opening mode. Thus, a comparison
 287 between the two failure modes is presented in figure 22.b in order to explain the
 288 trend of dissipated energy evolution with the loading angle.

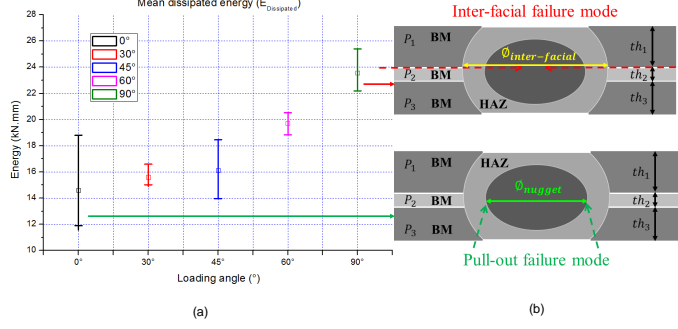


Figure 22: (a) Effect of the loading angle on the mean dissipated energy. (b) Illustrative scheme of the two failure modes

289 For the Pull-out failure mode, the rupture occurs around the spot weld
 290 nugget in the HAZ (where hardness has been measured at 300 Hv Figure; 20)
 291 with a Pull-out failure section equal to 14.45 mm², which can be calculated
 292 using Eq. 5.

$$S_{Pull-out} = \pi \times \phi_{nugget} \times th_3 \quad (5)$$

293 where $\phi_{Pull-out}$ is the nugget spot weld diameter and th_3 the P3 thickness
 294 (fig. 22).

295 However, for the Inter-facial failure mode, the rupture occurs at the interface
 296 P2/P1 across the nugget spot weld (where hardness has been measured at 460
 297 Hv) with a Inter-facial failure section equal to 50 mm², calculated using Eq. 6:

$$S_{Inter-facial} = \pi \times \phi_{Inter-facial}^2 / 4 \quad (6)$$

298 where $\phi_{Inter-facial}$ is the spot weld diameter (fig. 22).

299 The great difference in the failure cross-sections and material properties in
 300 the crack path explain the increase in dissipated energy when the loading angle
 301 increase.

302 4.2. Effect of the nugget spot weld diameter

303 Three nugget diameters are considered for the three-sheet spot welded
 304 assembly: 6.5 mm, 7.2 mm and 3.7 mm. They correspond respectively to the
 305 three lots, Lot 1, Lot 2 and Lot 3 (figure 2). Figure 23 presents the effect of the
 306 spot weld nugget diameter on the ultimate force and the dissipated energy. For a
 307 given loading angle, the ultimate force and the dissipated energy increase when
 308 the nugget spot weld diameter increases. These results present a good agreement
 309 with the published previous works [10, 11, 12, 13, 14, 15]. A significant combined
 310 effect of the loading angle and the nugget spot weld diameter is observed on the
 311 ultimate force and the dissipated energy. For instance, considering the two
 312 conform nugget spot welded specimens (Lot 1 and Lot 2), figure 23 shows no
 313 effect of the nugget spot weld diameter on the ultimate force and dissipated
 314 energy for $\psi = 0^\circ$, a small effect for $\psi = 30^\circ$ and a pronounced effect for $\psi =$
 315 90° .

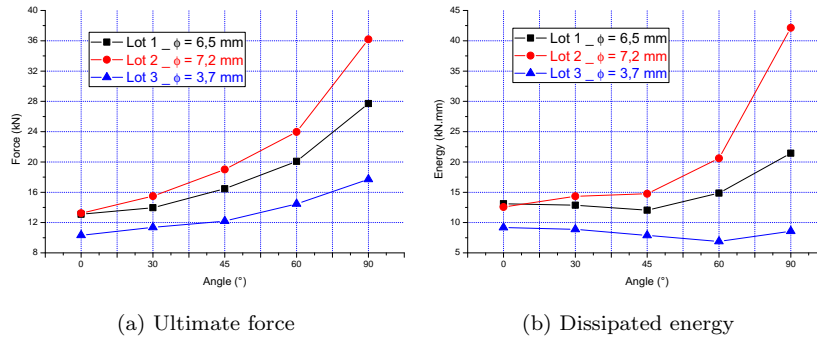


Figure 23: Effect of the nugget spot weld diameter on the (a) ultimate force and (b) dissipated energy

316 The effect of the nugget spot weld diameter is also highlighted in figure
 317 24) by superimposing the three rupture envelopes expressed by normal force
 318 component $N = \cos(\psi)$ vs. shear force component $S = \sin(\psi)$ for each lot.
 319 Whatever the loading angle, the dependency of the failure force to the spot
 320 weld diameter is obvious: the bigger the nugget, the higher the failure force.

321 Note that a force-based criterion of the form Eq. 7 [4] could be identified if
 322 required for each lot based on Figure 24.

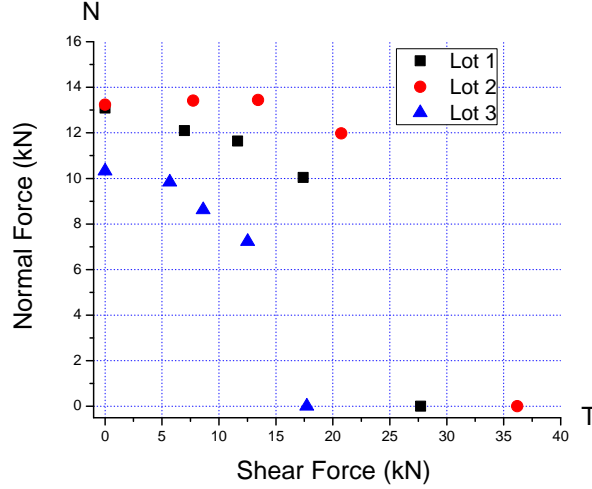


Figure 24: Effect of the nugget spot weld diameter on N-T diagram

$$\left(\frac{N}{N_u}\right)^a + \left(\frac{T}{T_u}\right)^b = 1 \quad (7)$$

323 where N_u is the ultimate normal force at failure obtained for $\psi = 0^\circ$, T_u
 324 is the ultimate tangential force at failure obtained for $\psi = 90^\circ$, a and b are
 325 exponents of the failure criterion identified from the experimental results of the
 326 combined loading tests.

327 5. Analysis of the dynamic loading sensitivity of three-sheet multi- 328 material spot welded assemblies

329 5.1. Strain rate effect on the base material (22MnB5)

330 The three sheet spot welded assembly is composed by two steel grades :
 331 22MnB5 ultra-high strength steel (UHSS) and DX54D mild steel. The DX54D
 332 mild steel grade is classified as an alloy quality low carbon steel. The mechanical
 333 behaviour and mechanical properties of the DX54D mild steel have been deeply

334 investigated on a large range of plastic strain rates and extensively reported
 335 in the literature. The 22MnB5 is classified as ultra-high strength steel. Its
 336 mechanical properties are extremely high comparing by DX54D mild steel.
 337 Table 5 presents the quasi-static mechanical properties of 22MnB5 and DX54D
 338 steels in terms of engineering stress and strain (data given by our industrial
 339 partner).

Table 5: 22MnB5 and DX54D base material properties

	22MnB5	DX54D
R_m - Tensile strength (MPa)	1500	260-360
R_e - 0.2% proof strength (MPa)	1100	120-220
A - Min. elongation $L_0 = 80$ mm (%)	34-36	6

340 The mechanical behaviour of the 22MnB5 base material is investigated under
 341 quasi-static and dynamic loadings in to order to check its strain rate sensitivity.

342 In the first step, quasi-static tests are realised using a high speed hydraulic
 343 machine (INSTRON VHS 65/20) with an imposed load speed $V_{QS} = 19 \times 10^{-3}$
 344 m/s. A good correlation is observed with the mechanical properties reported in
 345 table 5.

346 In the second step, dynamic tests are realised using a pre-stretched
 347 Hopkinson bars device. The pre-stretched bar technique is used her to acces
 348 to moderate strain rate, thus [100;1000] /s; Theses bars are made of mar-aging
 349 steel and composed of two cylindrical bars with 11 mm in diameter and 7 mm
 350 in length. The device is accurately aligned along a rigid I-beams frame and
 351 instrumented with strain gages so as to be calibrated as forces and velocities
 352 sensors. Details of equations, assumptions and analysis can be found in [16].
 353 Three impact velocities are applied as $V_D = 1.3$ m/s, 3.5 m/s and 5.65 m/s ($\dot{\epsilon}$
 354 (/s) = 125 , 350 and 550). Figure 25 presents the mean curves of the quasi-static
 355 stress vs. strain responses and the dynamic ones.

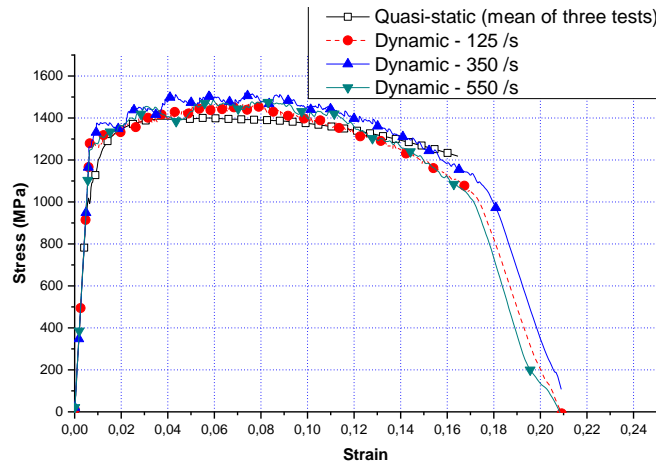


Figure 25: Strain rate effect of the base material 22MnB5 behaviour

356 The analysis of these curves shows two different tendencies. On the one
 357 hand, the hardening of the 22MnB5 UHSS base material is quite insensitive to
 358 the strain rate. On the other hand, the strain at failure seems to decrease with
 359 the strain rate. It can be related that the 22MnB5 UHSS base material is strain
 360 rate insensitive in the tested range.

361 5.2. Loading velocity sensitivity of the spot welded assembly

362 In a first step, it is proposed to evaluate the sensitivity of the assembly to
 363 the loading velocity in a low range by considering hydraulic jack experiment
 364 responses. A velocity jump of two decades ($V_1 = 0.001m/s$ and $V_2 = 0.1m/s$)
 365 and the angles $\psi = 0, 30$ and 60° are considered. No significant effect is
 366 observed on the ultimate force, displacement at failure, and energy (Figures
 367 26, 27)

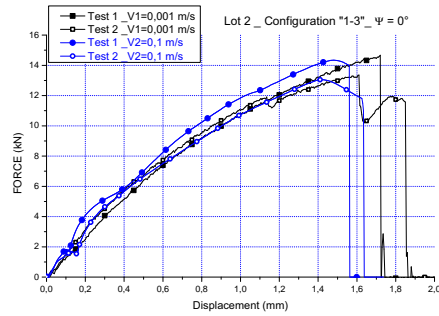


Figure 26: Loading velocity sensitivity under the pure opening load mode ($\psi = 0^\circ$)

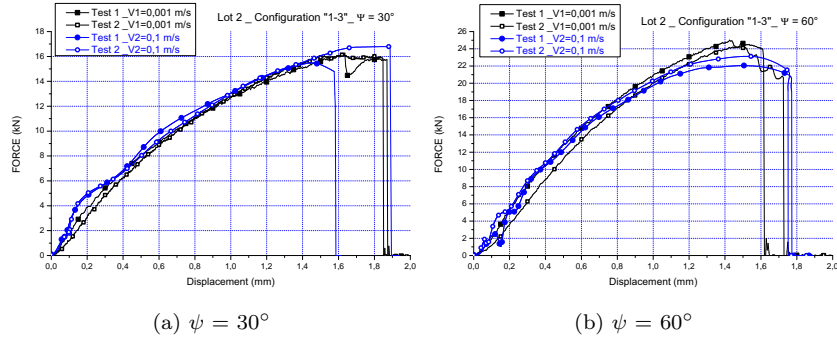


Figure 27: Loading velocity sensitivity under mixed modes (I/II) (a) $\psi = 30^\circ$ and (b) $\psi = 60^\circ$

368 In a second step it is proposed to evaluate the sensitivity of the assembly to
 369 the loading velocity in an higher range by comparing hydraulic jack experiment
 370 responses ($V_1 = 0.001m/s$ and $V_2 = 0.1m/s$) with Split Hopkinson Tension Bars
 371 experiment responses ($V_3 = 4m/s$) for a loading angle of $\psi = 0^\circ$.

372 A set of classical HSS bars used in tension thanks to a hollow projectile made
 373 of aluminium is proposed to test under dynamic condition a 3 sheets spot welds
 374 . The bars have a 30 mm diameter for a total length of 12 m. [17]

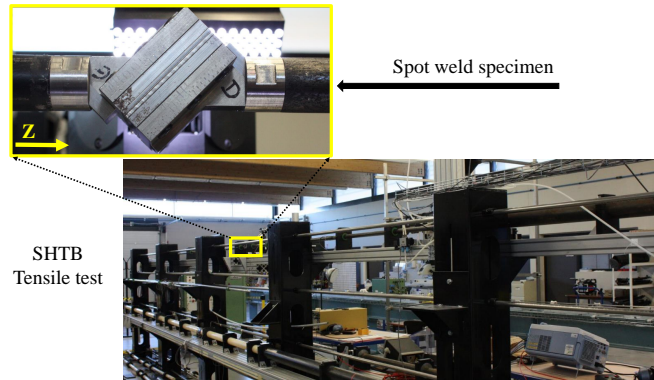


Figure 28: Split Hopkinson Tension Bars set-up for testing of spot-welded specimens under dynamic loading conditions

375 The raw signals of the SHTB tests are shown in Figure 29. The
 376 incident and transmitted waves are in accordance with what can be
 377 expected in classical data acquisition. However, the reflected wave
 378 reveals a peak which is expected to come from the section change
 379 caused by the mounting of the device along the bars. Thus this raw
 380 reflected signal cannot be considered as it is, and needs in fact to be
 381 rebuilt in accordance with the methodology presented in reference
 382 [16], i.e. considering a correct energy balance. In details, the reflected
 383 wave is rebuilt by subtraction of incident and transmitted waves. This
 384 new signal is used for the calculation of the specimen elongation. The
 385 transmitted wave which is less affected by the setup disturbances and
 386 the inertia effect is still used for the force calculation. The presented
 387 force-displacement curves related to the SHTB tests at $V_3 = 4m/s$ are
 388 following this methodology (figure 30).

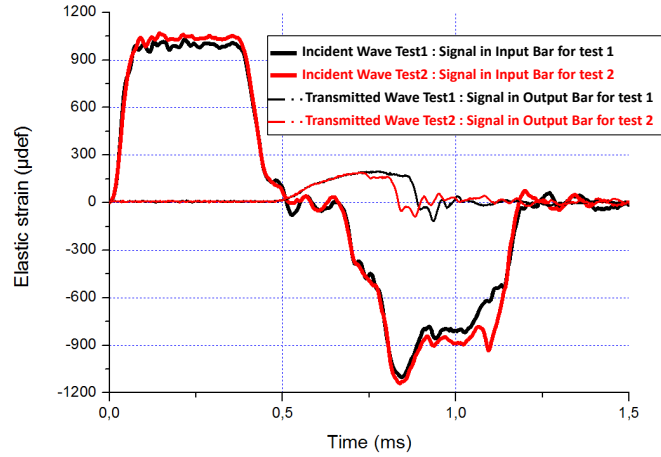


Figure 29: Raw signals from SHTB tests

389 Figure 30 compares the Force vs Displacement responses between quasi-
 390 static loading ($V_1 = 0.001m/s$) and both dynamic ones ($V_2 = 0.1m/s$ and
 391 $V_3 = 4m/s$) for pure opening mode.

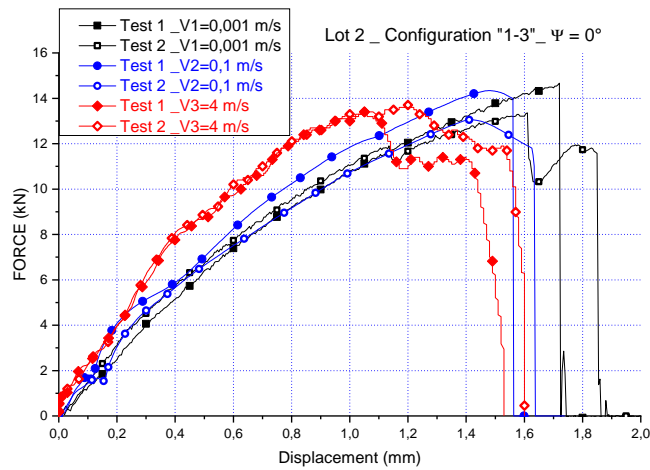


Figure 30: Loading velocity sensitivity under the pure opening load mode ($\psi = 0^\circ$) using SHTB system

392 No significant effect is reported on the ultimate force for pure opening mode.

393 This is in line with the rate insensitivity of the 22MnB5 constitutive material.
 394 An increase in the stiffness associated with a reduced displacement at failure,
 395 with iso energy by comparison with the lower loading velocities, suggests the
 396 existence of dynamic inertia effect. Other loading angles and higher velocities
 397 are however still necessary to confirm this preliminary suggestion.

398 Table 6 summarises ultimate forces, displacements at failure and dissipated
 399 energy for the different considered loading angles and velocities. These
 400 properties are presented in terms of mean values for each configuration and
 401 loading velocity.

Table 6: Mean values for ultimate forces, displacement at failure and dissipated energy for different loading angles and velocities

	Pure opening	Mixed opening/shear	
	$\psi = 0^\circ$	$\psi = 30^\circ$	$\psi = 60^\circ$
Ultimate force $V = 0.001m/s$ (kN)	13.95	16.08	24.54
Ultimate force $V = 0.1m/s$ (kN)	13.66	16.12	22.50
Ultimate force $V = 4m/s$ (kN)	13.55	–	–
Disp at failure $V = 0.001m/s$ (mm)	1.78	1.86	1.66
Disp at failure $V = 0.1m/s$ (mm)	1,60	1.75	1.76
Disp at failure $V = 4m/s$ (mm)	1.56	–	–
Dissipated energy $V = 0.001m/s$ (kN.mm)	15.92	19.70	26.50
Dissipated energy $V = 0.1m/s$ (kN.mm)	14.34	19.01	28.35
Dissipated energy $V = 4m/s$ (kN.mm)	14.70	–	–

402 6. Conclusion

403 The paper deals with the mechanical behaviour of multi-material multi-
 404 sheet spot welded assemblies and the failure modes under pure opening, pure
 405 shear, and mixed opening/shear modes. A three-sheet spot welded assembly
 406 combining two different steel grades (22MnB5 and DX54D) is considered with
 407 three weld nuggets diameters. The ultimate force, the displacement at failure
 408 and the dissipated energy are reported. A significant effect of the loading angle

409 is reported. This effect of the loading angle on the mechanical behaviour of the
410 spot welded assembly is explained through a comparison of the failure modes.
411 Three failure modes are identified : a pull-out failure mode (pure opening), an
412 inter-facial failure mode (pure Shear) and a mixed pull-out/inter-facial mode
413 (mixed opening/shear).

414 For each loading angle, three type of specimens with different spot weld
415 nugget size are tested. The analysis of force vs. displacement responses shows
416 that the nugget diameter has a significant effect on the ultimate force and the
417 dissipated energy. A significant combined effect of the loading angle and the
418 nugget spot weld diameter is observed on the mechanical response. Finally,
419 a preliminary study of the loading velocity sensitivity of the three-sheet spot
420 welded assembly is realized. No significant effect is reported on the ultimate
421 force for pure opening mode. However an increase in the stiffness associated
422 with a reduced displacement at failure suggests the existence of dynamic inertia
423 effect which has to be confirmed by a further intensive experimental campaign
424 with other loading angles and higher velocities. **Even if re design of the**
425 **set-up could minimise the dynamic inertia effect, it would be difficult**
426 **to cancel it completely. Moreover, considering the output bar signal**
427 **for the force calculation appears to give satisfying results, compared**
428 **to tests carried out at lower velocities on a hydraulic jack with a load**
429 **cell.**

430 **Acknowledgements**

431 The present research work has been supported by the European Community,
432 the Regional Delegation for Research and Technology, the French National
433 Research Agency, and by the Ministry of Higher Education and Research. The
434 authors gratefully acknowledge the support of these institutions.

435 **References**

- 436 [1] E. Hartmann, Mechanical tests of spot welds, *Welding Journal* 37,(1958),
437 520-523.
- 438 [2] D. J. VandenBossche, Ultimate Strength and Failure Mode of Spot welds
439 in High Strength Steels, SAE Technical Paper 770214, (1997).
- 440 [3] E. Markiewicz, P. Drazetic, Experimental and local/global numerical
441 characterization of mechanical strength for spot-welded assemblies,
442 *Mécanique et Industries* 4 (1), (2003), 17–27.
- 443 [4] Y.Lee, T. Wehner, M. Lu, T. Morrisett, E. Pakalnins, Ultimate strength
444 of resistance spot welds subjected to combined tension, *Journal of Testing
445 and Evaluation* 26 (3), (1998), 213–219.
- 446 [5] S. H. Lin, J. Pan, S.R. Wu, J. Tyan, P. Wung, Failure loads of spot welds
447 under combined opening and shear static loading conditions, *International
448 Journal of Solids and Structures* 39 (1), (2001), 19–39.
- 449 [6] S. H. Lin, J. Pan, J. Tyan, F. Prasad, A general failure criterion for spot-
450 welds under combined loading conditions, *International Journal of Solids
451 and Structures* 40 (21), (2004), 5539–5564.
- 452 [7] B. Langrand, A. Combescure, Non-linear and failure behaviour of
453 spotwelds: a global finite element and experiments in pure and mixed
454 modes I/II, *International Journal of Solids and Structures* 41 (24-
455 25),(2004), 6631–6646.
- 456 [8] B. Langrand, E. Markiewicz, Strain-rate dependence in spot welds: Non-
457 linear behaviour and failure in pure and combined modes I/II, *International
458 Journal of Impact Engineering* 37 (7), (2010), 792–805.
- 459 [9] J. H. Song, H. Huh, Failure characterization of spot welds under combined
460 axial–shear loading conditions, *International Journal of Mechanical
461 Sciences* 53 (7),(2011), 513 – 525.

- 462 [10] M. S. Pouranvari, M., Failure behavior of three-steel sheets resistance
463 spot welds : Effect of joint design, *Journal of Materials Engineering and*
464 *Performance* 21 (8), (2012), 1669–1675.
- 465 [11] M. S. Pouranvari, M., Weld nugget formation and mechanical properties of
466 three-sheet resistance spot welded low carbon steel, *The Canadian Journal*
467 *of Metallurgy and Materials Science* 51 (1), (2012), 105–110.
- 468 [12] A. Tavassolizadeh, P. Marashi, M. Pouranvari, Mechanical performance of
469 three thickness resistance spot welded low carbon steel, *Materials Science*
470 *and Technology* 27 (1), (2011), 219–224.
- 471 [13] C. Nielsen, K. Friis, W. Zhang, N. Bay, Three-sheet spot welding of
472 advanced high-strength steels, *Welding Research*, 90, (2011), 32–40.
- 473 [14] S. Wei, R. Liu, D. Lv, L. Lin, R. Xu, Y. Guo, Weldability and mechanical
474 properties of similar and dissimilar resistance spot welds of three-layer
475 advanced high strength steels, *Science and Technology of Welding and*
476 *Joining* 20 (1), (2015), 20–26.
- 477 [15] Y. Zhang, Y. Li, Z. Luo, Y. Feng, J. Zhou, Effect of joint design on the
478 failure behaviour of three-stack-up austenitic stainless steel resistance spot
479 welds, *Science and Technology of Welding and Joining* 21 (3), (2016), 484–
480 492.
- 481 [16] G. Haugou, N. Leconte, H. Morvan, Design of a pre-stretched tension
482 Hopkinson bar device: Configuration, tail corrections, and numerical
483 validation, *International Journal of Impact Engineering* 97, (2016), 89–101.
- 484 [17] G. Haugou, B. Bourel, F. Lauro, B. Bennani, D. Lesueur, D. Morin,
485 Characterization and modelling of structural bonding at high strain
486 rate, 10th International Conference on the Mechanical and Physical
487 Behaviour of Materials under Dynamic Loading, DYMAT, Freiburg,
488 Germany, september 2012, 7598-0757-4